Hyperbaric oxygen treatment improves pancreatic β-cell function and hepatic gluconeogenesis in STZ-induced type-2 diabetes mellitus model mice

CAISHUN ZHANG[1*], DI ZHANG[2*], HAIDAN WANG[1], QIAN LIN[1], MANWEN LI[1], JUNHUA YUAN[1], GUANGKAI GAO[1,3] and JING DONG[1,4]

[1]Special Medicine Department, College of Basic Medicine, Qingdao University, Qingdao, Shandong 266071; [2]Shandong Provincial Engineering Laboratory of Novel Pharmaceutical Excipients, Sustained and Controlled Release Preparations, College of Medicine and Nursing, Dezhou University, Dezhou, Shandong 253023; [3]Department of Hyperbaric Medicine, No. 971 Hospital of Chinese People's Liberation Army; [4]Physiology Department, College of Basic Medicine, Qingdao University, Qingdao, Shandong 266071, P.R. China

Received July 6, 2021; Accepted October 14, 2021

DOI: 10.3892/mmr.2022.12606

Abstract. Type-2 diabetes mellitus (T2DM) causes several complications that affect the quality of life and life span of patients. Hyperbaric oxygen therapy (HBOT) has been used to successfully treat several diseases, including carbon monoxide poisoning, ischemia, infections and diabetic foot ulcer, and increases insulin sensitivity in T2DM. The present study aimed to determine the effect of HBOT on β-cell function and hepatic gluconeogenesis in streptozotocin (STZ)-induced type-2 diabetic mice. To establish a T2DM model, 7-week-old male C57BL/6J mice were fed a high-fat diet (HFD) and injected once daily with low-dose STZ for 3 days after 1-week HFD feeding. At the 14th week, HFD+HBOT and T2DM+HBOT groups received 1-h HBOT (2 ATA; 100% pure O_2) daily from 5:00 to 6:00 p.m. for 7 days. The HFD and T2DM groups were maintained under normobaric oxygen conditions and used as controls. During HBOT, the 12-h nocturnal food intake and body weight were measured daily. Moreover, blood glucose was measured by using a tail vein prick and a glucometer. After the final HBO treatment, all mice were sacrificed to conduct molecular biology experiments. Fasting insulin levels of blood samples of sacrificed mice were measured by an ultrasensitive ELISA kit. Pancreas and liver tissues were stained with hematoxylin and eosin, while immunohistochemistry was performed to determine the effects of HBOT on insulin resistance. TUNEL was used to determine the effects of HBOT on β-cell apoptosis, and immunoblotting was conducted to determine the β-cell apoptosis pathway. HBOT notably reduced fasting blood glucose and improved insulin sensitivity in T2DM mice. After HBOT, β-cell area and β-cell mass in T2DM mice were significantly increased. HBOT significantly decreased the β-cell apoptotic rate in T2DM mice via the pancreatic Bcl-2/caspase-3/poly(ADP-ribose) polymerase (PARP) apoptosis pathway. Moreover, HBOT improved the morphology of the liver tissue and increased hepatic glycogen storage in T2DM mice. These findings suggested that HBOT ameliorated the insulin sensitivity of T2DM mice by decreasing the β-cell apoptotic rate via the pancreatic Bcl-2/caspase-3/PARP apoptosis pathway.

Introduction

With the improvement of living standards, the occurrence of metabolic diseases, such as diabetes, is increasing. Diabetes is a multifactorial and chronic disease that occurs when the body cannot produce enough insulin or use insulin effectively, resulting in elevated blood glucose levels (1). Type-2 diabetes mellitus (T2DM) is a common type of diabetes. Hyperglycemia is the result of insulin resistance and pancreatic β-cell dysfunction (2). Pancreatic β-cells respond to increased blood glucose levels by secreting insulin; however, in T2DM, there is a loss of β-cells (3). DeFronzo *et al* (4) showed that β-cell function was reduced by >80% in patients with impaired glucose tolerance and was decreased further in patients with T2DM. Regulation of β-cell mass occurs by balancing the formation of new β-cells and the loss of β-cells (5). Butler *et al* (6) reported that β-cell apoptosis was increased in T2DM, which may cause β-cell dysfunction.

Hyperbaric oxygen therapy (HBOT) is the process by which a patient or animal receives 100% oxygen at pressures >1 atmosphere. HBOT has been used to successfully treat numerous conditions, including carbon monoxide poisoning,

Correspondence to: Professor Jing Dong, Physiology Department, College of Basic Medicine, Qingdao University, Medical Education Building C, 16 Ning De Road, Qingdao, Shandong 266071, P.R. China
E-mail: dongjing6@hotmail.com

*Contributed equally

Key words: hyperbaric oxygen, β-cell apoptosis, Bcl-2/caspase-3/poly(ADP-ribose) polymerase pathway, type-2 diabetes mellitus

ischemia, infections and wounds (7). As for wound care, HBOT can accelerate diabetic foot ulcer healing in patients with diabetes mellitus by increasing oxygen dispersion to damaged tissues, alleviating inflammation and suppressing the growth of anaerobic bacteria (8,9). In patients with diabetic foot, HBOT has also been shown to have beneficial effects on glycemic control (8). Moreover, HBOT reduces fasting blood glucose levels and increased insulin sensitivity (10,11). In T2DM, the mechanism involves increased skeletal muscle oxidative capacity (12). Our previous study demonstrated that HBOT improved insulin sensitivity by activating Akt protein phosphorylation to promote glucose transporter type 4 (GLUT4) expression in T2DM, resulting in reduced blood glucose levels (13).

However, the effects of HBOT on β-cell function have not been fully studied. Although islet cells account for a small amount of the total weight of the pancreas, they consume ~10% of the total pancreatic blood flow (14). As HBOT increases oxygen content in the blood flow, the present study aimed to investigate whether HBOT could ameliorate insulin resistance by acting on β-cells.

Materials and methods

Animals and food. Adult male C57BL/6J mice (age, 6 weeks; weight, 15-18 g) were obtained from Qingdao Institute Food and Drug Control and housed in standard rodent cages. Animals were housed in a temperature-controlled (23±2˚C) and humidity-controlled (55±20%) animal room (illumination from 7:00 to 19:00) with free access to standard food and tap water for at least 1 week to adapt to their surroundings. The experimental protocols were approved by the Qingdao University Animal Care and Use Committee and Animal Welfare Committee (approval no. QYFY WzLL26594).

After 1 week of acclimatization, the 7-week-old mice were fed a high-fat-diet (HFD) consisting of 59% basic mice feed, 20% sugar, 18% lard and 3% egg yolk.

Experimental groups and HBOT. The 24 adult male C57BL/6J mice were randomly divided into the following four groups: i) HFD (n=4); ii) HFD+HBOT (n=4); iii) T2DM (n=8); and iv) T2DM+HBOT (n=8). Following the contrast principle and the single variable principle, the T2DM and T2DM+HBOT groups were used as the experimental groups, whereas the HFD and HFD+HBOT groups were used as the control groups. As the expected success rate of T2DM modeling was unknown at first, the sample size of the T2DM group was doubled in order to reduce sampling error and improve statistical efficiency. As the results showed that the rate of successful T2DM model establishment was 100%, the sample sizes of the HFD and T2DM groups were 4 and 8, respectively.

From the 7th week, all mice were fed a HFD until sacrifice. HFD feeding was combined with a subsequent injection of low-dose streptozotocin (STZ, 60 mg/kg; i.p.; cat. no. S0130; Sigma-Aldrich; Merck KGaA) to model T2DM. Young adult mice are fed a HFD to elicit insulin resistance, multiple injections with low-dose STZ then elicit partial loss of β-cells, which results in hypoinsulinemia and hyperglycemia (15). T2DM mice were intraperitoneally injected with low-dose STZ once daily for 3 days after 1-week HFD feeding. The age-matched HFD mice were injected with the same frequency citrate buffer as STZ alone (15,16). Mice with fasting blood glucose levels >12 mmol/l were defined as successful T2DM models (13).

At the 14th week, HFD+HBOT and T2DM+HBOT groups received 1-h HBOT daily from 5:00 to 6:00 p.m. for 7 days, whereas the other two groups received normobaric oxygen in the same chamber. HBOT was administered in an animal HBO chamber (Moon Environmental Technology Co., Ltd.), operating at high pressure (2 ATA) with 100% oxygen, including a 5-min pressure rise adaptation stage, 50-min stabilization stage and 5-min re-pressurization stage (17). After the final HBOT, an intraperitoneal glucose tolerance test (IPGTT) was performed. Subsequently, the mice were sacrificed by exsanguination following an intraperitoneal injection of 50 mg/kg sodium pentobarbital. Blood samples were obtained from the orbital sinus and stored at -20˚C or -80˚C until further use (18,19).

Food intake and body weight. As mice are primarily nocturnal and their feeding activity typically occurs during the night, nocturnal food intake was assessed (20). During HBOT, the 12-h nocturnal food intake was measured daily to investigate the effects of HBOT on nocturnal food intake (20). An electronic precision scale (TE412-L; Sartorius AG) was used to weigh the food at 8:00 a.m and 8:00 p.m. The 12-h nocturnal food intake was defined as the weight of the food at 8:00 p.m. minus the weight of the food at 8:00 a.m. the following morning. An electric balance (PL1501-S; Mettler Toledo) was used to weigh the mice at 8:00 a.m. after weighing the food.

Blood glucose, intraperitoneal glucose tolerance test (IPGTT) and insulin level. To determine the success of T2DM model establishment, non-fasting blood glucose (non-FBG) was measured after 42 days of STZ injection by a tail vein prick and a glucometer.

Before HBOT, fasting blood glucose (FBG) levels were measured in the four groups and then FBG levels were assessed again after 7-day HBOT to observe the effects of HBOT on FBG.

FBG was measured at 9:00 a.m. after a 12-h fast and non-FBG was measured at 2:00 p.m. without fasting.

The IPGTT was performed in the T2DM and T2DM+HBOT groups after 7-day HBOT. The mice were allowed to fast for 14 h before the IPGTT and then intraperitoneally administered glucose (2 g/kg body weight). Using a glucometer, blood glucose concentrations were measured at 0, 15, 30, 60, 90 and 120 min after IPGTT using tail vein blood.

Fasting insulin (FI) levels of the blood samples obtained from sacrificed mice were measured using an ultrasensitive ELISA Kit (cat. no. CEA448Ra, Wuhan USCN Business Co., Ltd.). The homeostasis model assessment for insulin resistance and β-cell function (HOMA-IR and HOMA-β, respectively) indices were also measured (21). The HOMA-IR was calculated as follows: FI (mU/ml) x FBG (mmol/l)/22.5. The HOMA-β was calculated as follows: 20 x FI/(FBG-3.5) (22).

Fat mass and pancreas weight. Electronic precision scales were used to measure fat mass, including inguinal adipose tissue, epididymal adipose tissue and pancreas weight. The sum of the inguinal white adipose tissue (iWAT) weight and epididymal white adipose tissue (eWAT) weight was calculated to assess the total weight of the fat pad, reflecting the balance of fat accumulation and metabolism. The current study calculated the pancreas weight coefficient as follows: Pancreas weight/body weight on the 8th day.

Hematoxylin and eosin (H&E) staining. Pancreatic and liver tissues were fixed in 4% formaldehyde at 4˚C for 24 h. After dehydration with various ethanol concentrations (75, 80, 85, 95 I, 95 II, 100 I and 100% II, 5 min each at room temperature) and clarifying with xylene (xylene I and xylene II, 10 min each at room temperature), the tissues were embedded in soft paraffin, hard paraffin and mixed paraffin (1 h for each) before sectioning, the temperature was 2-3˚C above the melting point, at last the tissues were solidified in the mixed paraffin at room temperature. After sectioning into 4-6-μm sections using a paraffin slicing machine (RM2016; Leica Microsystems, Inc.), the tissue sections were stained using a hematoxylin-eosin staining kit (cat. no. C0105; Beyotime Institute of Biotechnology). The light microscope (CX31; Olympus Corporation) was used to observe staining results. Cell numbers were counted using ImageJ software (version 1.8.0; National Institutes of Health).

Immunohistochemistry. Paraffin-embedded sections (thickness, 4-6-μm) were used to determine the effects of HBOT on insulin resistance. Pancreatic tissues were fixed in 4% formaldehyde at 4˚C for 24 h. After dehydration with various ethanol concentrations (5 min each at room temperature) and clarifying with xylene (xylene I and xylene II, 10 min each at room temperature), the tissues were embedded in soft paraffin, hard paraffin and mixed paraffin (1 h for each) before sectioning, the temperature was 2-3˚C above the melting point, lastly the tissues were solidified in the mixed paraffin at room temperature. After sectioning, the tissues were dewaxed by xylene for (xylene I and xylene II) 10 min each at room temperature and placed in different ethanol concentrations (100 I, 100 II, 95 I, 95 II, 85, 80 and 75%) for 5 min each at room temperature. Following antigen retrieval by heating at 95˚C in citrate buffer for 1 h, the sections were quenched with 0.3% hydrogen peroxide at room temperature for 30 min. After three washes in 0.01 M PBS, the sections were blocked with 1% BSA (cat. no. 1213G057; Beijing Solarbio Science & Technology Co., Ltd.) in 0.01 M PBS for 1 h at 37˚C. Subsequently, the sections were incubated with a rabbit anti-insulin primary antibody (1:200; cat. no. 4590; Cell Signaling Technology, Inc.) overnight at 4˚C. The sections were then incubated with a HRP-conjugated secondary antibody (cat. no. ZB2301; Zsbio; http://www.zsbio.com/product/ZB-2301) for 3 h at 37˚C. Finally, 3,3'diaminobenzidine (DAB) staining was performed using a kit (cat. no. ZLI-9018; Zsbio) according to the manufacturer's protocol. The nuclei were stained for 30 sec to 1 min, then the sections were rinsed with running water for 10 min. Differentiation: 70, 90, 100 I, 100% II ethanol, xylene I and xylene II, 2 min each at room temperature. The slides were removed from xylene and neutral gum was used to seal the slides. The morphology was assessed using a CX31 light microscope (Olympus Corporation). The β-cell area ratio was assessed using Image-Pro Plus software (Version 6.0, Media Cybernetics, Inc.). The β-cell mass was calculated by the β-cell area ratio and pancreas weight (23,24): β-cell mass=β-cell area ratio x pancreas weight.

TUNEL assay. Paraffin-embedded sections (thickness, 4-6-μm) were used to determine the effects of HBOT on β-cell apoptosis. Pancreatic tissues were fixed in 4% formaldehyde at 4˚C for 24 h. After dehydration with various ethanol concentrations (5 min each at room temperature) and clarifying with xylene (xylene I and xylene II, 10 min each at room temperature), the tissues were embedded in soft paraffin, hard paraffin and mixed paraffin (1 h for each) before sectioning, the temperature was 2-3˚C above the melting point, lastly the tissues were solidified in the mixed paraffin at room temperature. After sectioning, the tissues were dewaxed by xylene (xylene I and xylene II) for 20 min each and placed in different ethanol concentrations (100 I, 100 II, 95 I, 95 II, 85, 80 and 75%) for 5 min each at room temperature, then the tissues were incubated in 0.1% Triton for 10 min. After four washes with PBS (2 min per wash), the sections were incubated with protease K (20 μg/ml in 10 mM Tris-HCl, pH 8.0) and digested for 15 min. Subsequently, the sections were incubated in labeling buffer for 2 h at 37˚C. After rinsing three times with PBS, the sections were stained using a TUNEL Cell Apoptosis Detection kit III (FITC, cat. no. MK1023; Boster Biological Technology) according to the manufacturer's protocol. Sections were also immunostained with anti-insulin antibody to identify β-cells, they were incubated with a rabbit anti-insulin primary antibody (1:200; cat. no. 4590; Cell Signaling Technology, Inc.) overnight at 4˚C and incubated with a HRP-conjugated secondary antibody (cat. no. ZB2301; Zsbio) for 3 h at 37˚C. The slides were rinsed in 0.01 M PBS buffer and mounted in fluorescent mounting medium (Dako; Agilent Technologies, Inc.). Differentiation: 70, 90, 100 I, 100% II ethanol, xylene I and xylene II, 2 min each at room temperature. The slides were removed from xylene and neutral gum was used to seal the slides. The stained sections were visualized using a fluorescence microscope and apoptotic cell numbers were counted using ImageJ software (version 1.8.0; National Institutes of Health). In total, 20 islets were chosen at random from each group of individual mice.

Western blotting. Total protein was isolated from pancreatic tissues using RIPA buffer (cat. no. P0013B; Beyotime Institute of Biotechnology) supplemented with protease inhibitors (1:100; cat. no. P1005; Beyotime Institute of Biotechnology). After centrifugation at 14,000 x g for 10 min (4˚C), protein concentrations were determined using a BCA assay (cat. no. P0012; Beyotime Institute of Biotechnology). Proteins were denatured in sodium dodecyl sulfate sampling buffer (95˚C for 5 min), then separated using 12% polyacrylamide gel electrophoresis. After transferring to PVDF membranes (cat. no. IPVH00010, MilliporeSigma) over 2 h, the membranes were blocked with 5% FBS (cat. no. 9048-46-8, Beijing Solarbio Science & Technology Co., Ltd.) for 2 h at room temperature. The mass of protein was 30 μg/12 μl per lane. Subsequently, the membranes

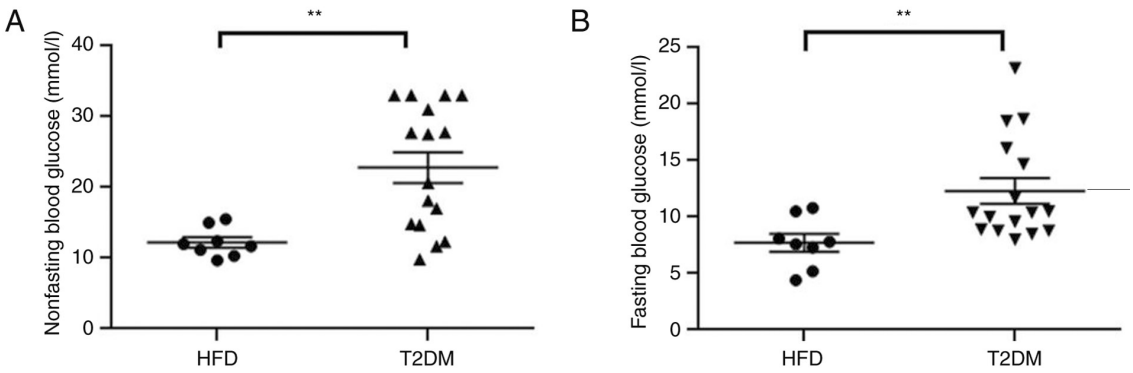

Figure 1. Blood glucose levels after streptozotocin injection in T2DM mice. (A) Non-fasting blood glucose and (B) fasting blood glucose levels in the T2DM and HFD groups. Data are presented as the mean ± SEM. **P<0.01. T2DM, type-2 diabetes mellitus; HFD, high-fat diet.

were incubated at 4˚C overnight with primary antibodies targeted against the following: Bax (rabbit IgG; cat. no. 2772; 1:2,000; Cell Signaling Technology, Inc.), Bcl-2 (rabbit IgG; cat. no. ab196495; 1:2,000; Abcam), caspase-3 (Casp-3, rabbit IgG; cat. no. ab184787; 1:2,000; Abcam), cleaved Casp-3 (rabbit IgG; cat. no. ab214430; 1:2,000; Abcam), poly(ADP-ribose) polymerase (PARP; rabbit IgG; cat. no. 9532; 1:2,000; Cell Signaling Technology, Inc.), cleaved PARP (rabbit IgG; cat. no. 5625; 1:2,000; Cell Signaling Technology, Inc.) and β-actin (rabbit IgG; cat. no. 4967; 1:4,000; Cell Signaling Technology, Inc.). The membranes were then incubated with a goat anti-rabbit IgG H&L HRP-conjugated secondary antibody (cat. no. ab6721; 1:2,000; Abcam) at room temperature for 1 h. Protein bands were visualized using Immobilon western chemiluminescent substrate (cat. no. WBKLS0100; 200 μl; MilliporeSigma) and a UVP 810 gel-imager (Analytik Jena AG). Protein expression was semi-quantified using ImageJ software (version 1.8.0, National Institutes of Health).

Statistical analysis. The experiments were repeated >2 times. Data are presented as the mean ± SEM. Comparisons between two groups were analyzed using the unpaired Student's t-test. Comparisons among multiple groups were analyzed using one-way ANOVA followed by Tukey's post hoc test. GraphPad Prism (GraphPad Software, Inc, version 7.0.) and SPSS (SPSS Inc, version 22.0) software were used to create graphs and perform statistical analyses. P<0.05 was considered to indicate a statistically significant difference.

Results

Establishment of the T2DM mouse model. Non-FBG was measured for 2 consecutive days after 42 days injecting low-dose STZ (Fig. 1A). FBG was measured before the HBO intervention (Fig. 1B). Both the non-FBG (22.81±1.88 vs. 12.23±0.73 mmol/l; P<0.01) and FBG (12.30±1.14 vs. 7.71±0.79 mmol/l; P<0.01) levels of the T2DM group were significantly higher compared with those in the HFD group, which indicated successful establishment of the T2DM model. No mice died during the model establishment and the successful T2DM model establishment rate was 100%.

Effects of HBOT on nocturnal feeding and body weight in T2DM mice. During HBOT, all mice were fed separately for 7 days and their 12-h nocturnal feeding and body weight were assessed daily. There were no marked differences among the HBOT groups in 12-h nocturnal food intake (P>0.05; Fig. 2A). The body weight appeared to increase at first, then decrease; however, there were no significant differences among the four groups (P>0.05; Fig. 2B). Body weight gain after HBO intervention was determined on the 8th day, and the results indicated that HBOT did not reduce body weight gain in both the HFD (1.292±0.021 vs. 0.922±0.19 g; P>0.05) and T2DM (1.164±0.102 vs. 0.891±0.059 g; P>0.05) groups (Fig. 2C).

Effects of HBOT on blood glucose and insulin sensitivity in T2DM mice. HBOT notably reduced FBG in T2DM mice (11.63±1.26 vs. 8.11±0.74 mmol/l; P>0.05; Fig. 3A). The glucose tolerance tests showed that HBOT significantly reduced peak blood glucose levels at 15 min (21.48±2.88 vs. 14.26±2.51; P<0.05; Fig. 3B) and the area under the blood glucose curve within 120 min of IPGTT (1,628±185 vs. 1,425±72; P<0.05; Fig. 3C) in T2DM mice, suggesting that HBOT reduced FBG levels and improved glucose tolerance in T2DM.

To assess insulin resistance and β-cell function, HOMA-IR and HOMA-β were calculated. The HOMA-IR of T2DM mice was significantly higher compared with that of HFD mice (8.98±0.55 vs. 2.96±0.27; P<0.001). There were no significant differences between the two HFD groups (2.96±0.272 vs. 3.25±0.12; P>0.05). Compared with the T2DM group, the HOMA-IR was significantly reduced in the T2DM+HBOT group (8.98±0.55 vs. 6.17±0.21; P<0.01; Fig. 3D). The HOMA-β of T2DM mice was significantly lower compared with that in the HFD group (0.362±0.84 vs. 1.084±0.102; P<0.01). Moreover, there was no significant difference between the two HFD groups or between the two T2DM groups (P>0.05; Fig. 3E).

Effects of HBOT on fat pad and pancreas weight in T2DM mice. Visceral adipose tissue and subcutaneous adipose tissue are considered as distinct types of white fat. Typically, the inguinal fat weight is measured to reflect subcutaneous adipose tissue and the epididymal fat weight is measured to reflect visceral adipose tissue (25,26). Therefore, the weights of visceral epididymal fat and inguinal subcutaneous fat were measured in the present study.

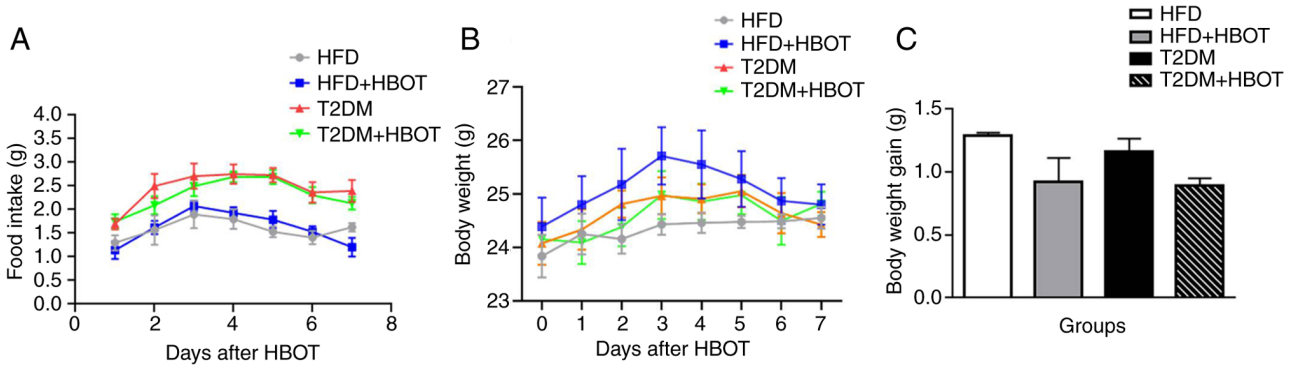

Figure 2. Effects of HBOT on nocturnal feeding, body weight and body weight gain. Effects of 7-day HBOT on (A) nocturnal food intake and (B) body weight. (C) HBO-induced body weight gain after 7-day HBO intervention. Data are presented as the mean ± SEM. HBO, hyperbaric oxygen; HFD, high-fat diet; T2DM, type-2 diabetes mellitus; HBOT, hyperbaric oxygen therapy.

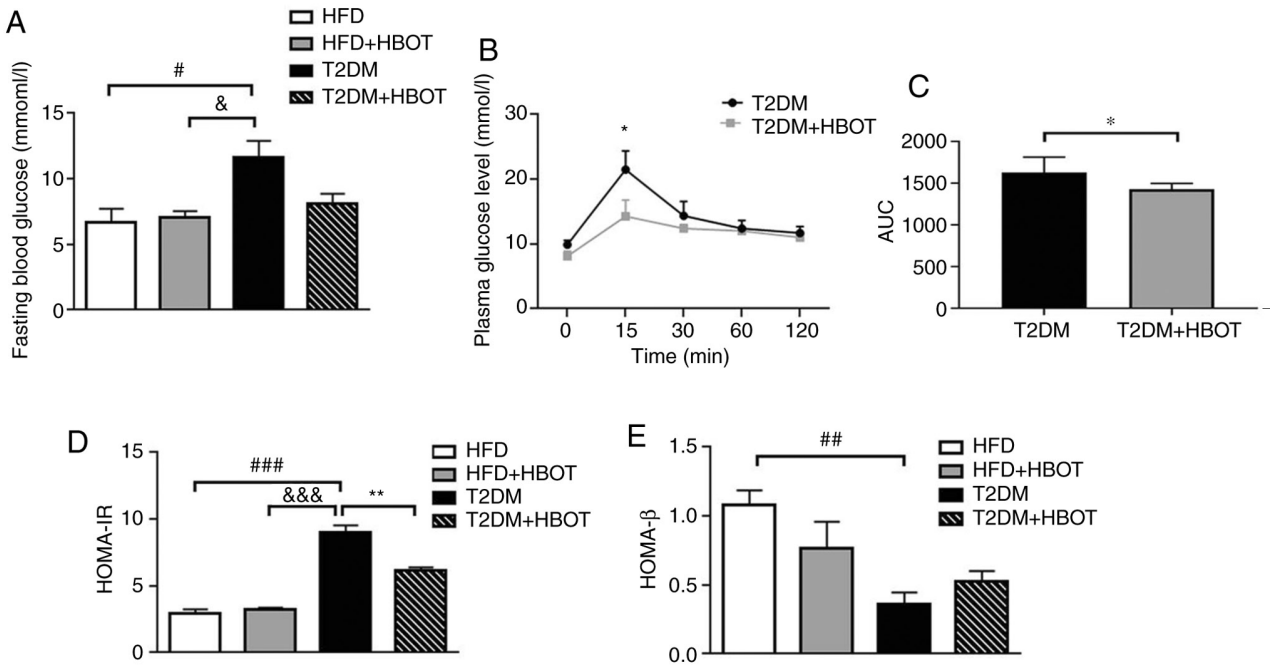

Figure 3. Effects of HBOT on blood glucose and insulin sensitivity. (A) Fasting blood glucose pre- and post-7-day HBOT. (B) Intraperitoneal glucose tolerance test in T2DM mice after 7-day HBOT. (C) AUC in the T2DM and T2DM+HBOT groups after 7-day HBOT. (D) HOMA-IR and (E) HOMA-β values in the HFD and T2DM groups. Data are presented as the mean ± SEM. *P<0.05 and **P<0.01; $^{\#}$P<0.05, $^{\#\#}$P<0.01 and $^{\#\#\#}$P<0.001; $^{\&}$P<0.05 and $^{\&\&\&}$P<0.001. HBO, hyperbaric oxygen; T2DM, type-2 diabetes mellitus; AUC, area under the blood glucose curve; HOMA-IR, homeostatic model assessment of insulin resistance; HOMA-β, homeostatic model assessment of β-cell function; HFD, high-fat diet; HBOT, hyperbaric oxygen therapy.

The weight of the inguinal subcutaneous adipose tissue was significantly lower in the T2DM+HBOT group compared with that in the T2DM group (0.311±0.019 vs. 0.451±0.034 g; P<0.01; (Fig. 4A), although there was no significant difference in the weight of the visceral epididymal adipose tissue between these two T2DM groups (P>0.05; Fig. 4B). HBOT significantly decreased the sum of iWAT and eWAT weight in T2DM mice (0.592±0.049 vs. 0.856±0.067 g; P<0.05; Fig. 4C). Compared with the T2DM group, the pancreas weight (0.206±0.012 vs. 0.143±0.004 g; P<0.01) and the pancreas weight coefficient were significantly increased in the T2DM+HBOT group (0.849±0.053 vs. 0.582±0.026; P<0.01; Fig. 4D and E).

Effects of HBOT on pancreas β-cell morphology and structure in T2DM mice. The islets were divided into large and small islets; those with >10 islet cells were defined as large islets and those with ≤10 cells as small islets.

H&E staining showed that the number of small islets was higher, whereas the number of large islets was lower in the T2DM group compared with the HFD group. After HBOT, the number of large islets increased significantly in T2DM mice (0.52±0.016 vs. 0.42±0.019; P<0.01; Fig. 5A).

The β-cell area in the T2DM group was significantly smaller compared with that in the HFD (3.77±0.38 vs. 6.097±0.88; P<0.05) and HFD+HBOT (3.77±0.38 vs. 8.77±1.18; P<0.05) groups. After HBOT, the β-cell area in T2DM mice was significantly increased (3.77±0.38 vs. 7.68±1.68; P<0.05), albeit smaller compared with that in the HFD and HFD+HBOT groups (Fig. 5B). In the T2DM mice, the β-cell mass was significantly lower in pancreatic tissue compared

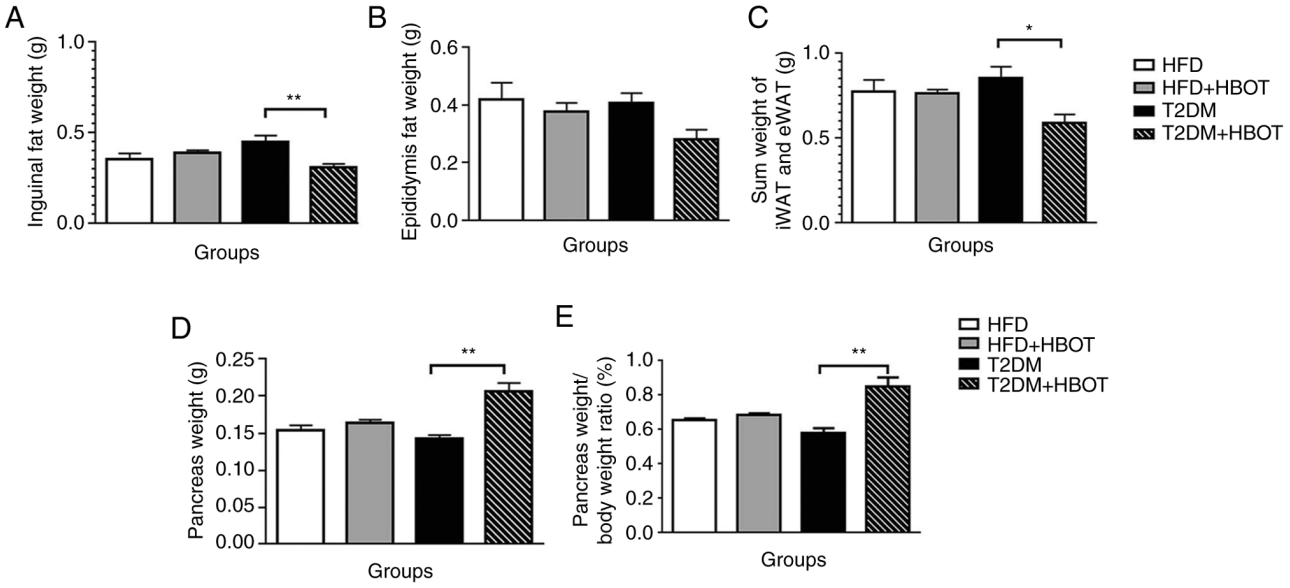

Figure 4. Effects of HBOT on fat and pancreas weight. Effects of HBOT on the weight of (A) inguinal fat, (B) epididymal fat and (C) the sum weight of the inguinal fat and epididymal fat. (D) Pancreas weight in T2DM mice and HFD mice. (E) Ratio of pancreas weight to the 8th body weight. Data are presented as the mean ± SEM. *P<0.05 and **P<0.01. HBO, hyperbaric oxygen; T2DM, type-2 diabetes mellitus; HFD, high-fat diet; HBOT, hyperbaric oxygen therapy; iWAT, inguinal white adipose tissue; eWAT, epididymal white adipose tissue.

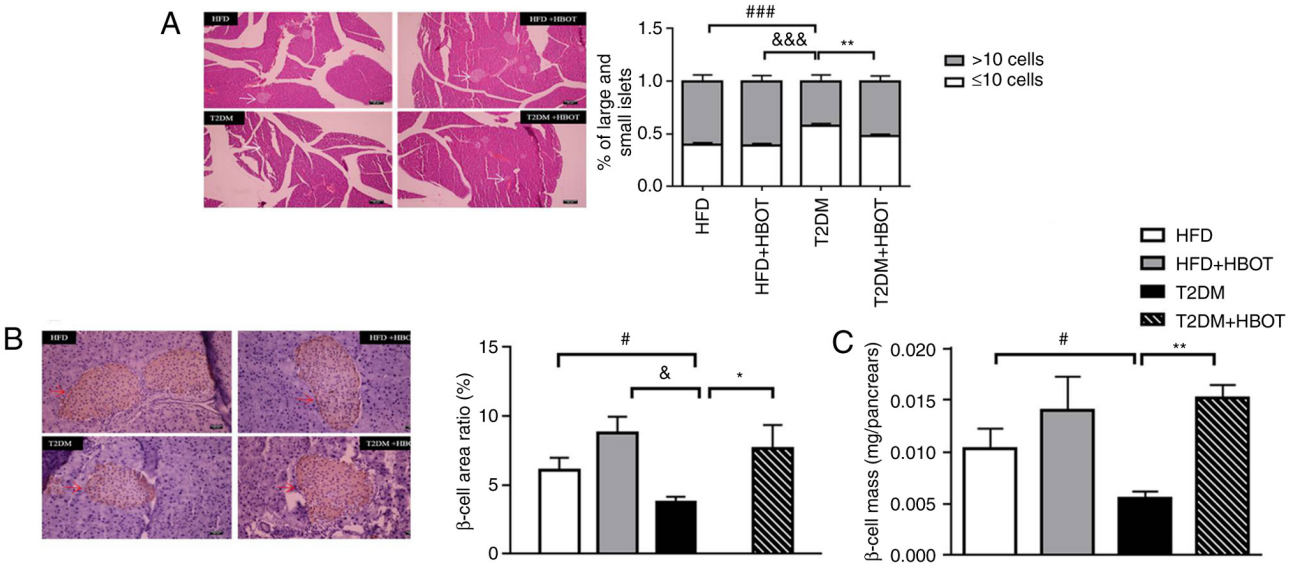

Figure 5. Effects of HBOT on pancreatic β-cell morphology and structure. (A) H&E staining of the pancreas (scale bar, 68 μm). Effects of HBOT on the number of islets. (B) Representative immunohistochemistry images of insulin staining in pancreatic tissues (Scale bar, 142 μm). Effects of HBOT on β-cell area. (C) Effects of HBOT on β-cell mass. Data are presented as the mean ± SEM. *P<0.05 and **P<0.01; $^{\#}$P<0.05 and $^{\#\#\#}$P<0.001; $^{\&}$P<0.05 and $^{\&\&\&}$P<0.001. HBO, hyperbaric oxygen; HFD, high-fat diet; HBOT, hyperbaric oxygen therapy; T2DM, type-2 diabetes mellitus.

with the HFD group (0.0103±0.0019 vs. 0.005463±0.000691; P<0.05). However, HBOT significantly increased β-cell mass by ~2-fold without HBOT in T2DM mice (0.005463±0.000691 vs. 0.015201±0.001261; P<0.01; Fig. 5C).

Effects of HBOT on pancreas β-cell apoptosis in T2DM mice. The TUNEL results showed that HBOT significantly reduced the β-cell apoptotic rate in T2DM mice (0.3588±0.01237 vs. 0.1550±0.00898; P<0.001; Fig. 6A).

To further investigate the mechanism underlying HBO-mediated inhibition of β-cell apoptosis, the expression levels of the apoptosis-related proteins Bax/Bcl-2, caspase-3 and downstream PARP were measured in pancreatic tissue. After HBOT, the expression levels of Bax were markedly decreased, whereas Bcl-2 expression levels were notably increased, resulting in a significantly decreased Bax/Bcl-2 ratio in T2DM mice. The expression levels of cleaved caspase-3 and cleaved PARP were significantly lower in the T2DM+HBOT group compared with those in the T2DM group (Fig. 6B).

Effects of HBOT on hepatic gluconeogenesis in T2DM mice. H&E staining showed that the arrangement cords of

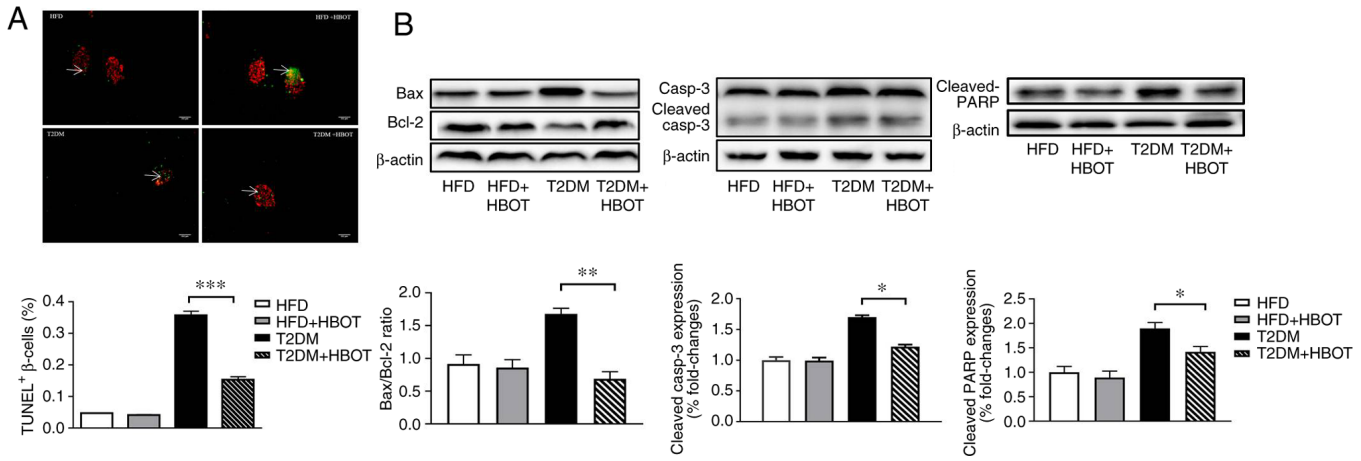

Figure 6. Effects of HBOT on β-cell apoptosis. (A) TUNEL staining of β-cell apoptosis. Red fluorescence indicates pancreatic β-cells and green fluorescence indicates apoptotic cells (scale bar, 252 μm), white arrows indicate TUNEL$^+$ β-cells (%). (B) Effects of HBOT on the expression levels of apoptosis-related proteins, including Bax/Bcl-2, Casp-3 and PARP, in pancreatic tissue. Data are presented as the mean ± SEM. *P<0.05, **P<0.01 and ***P<0.001. HBO, hyperbaric oxygen; PARP, poly(ADP-ribose) polymerase; HFD, high-fat diet; HBOT, hyperbaric oxygen therapy; T2DM, type-2 diabetes mellitus; Casp, caspase.

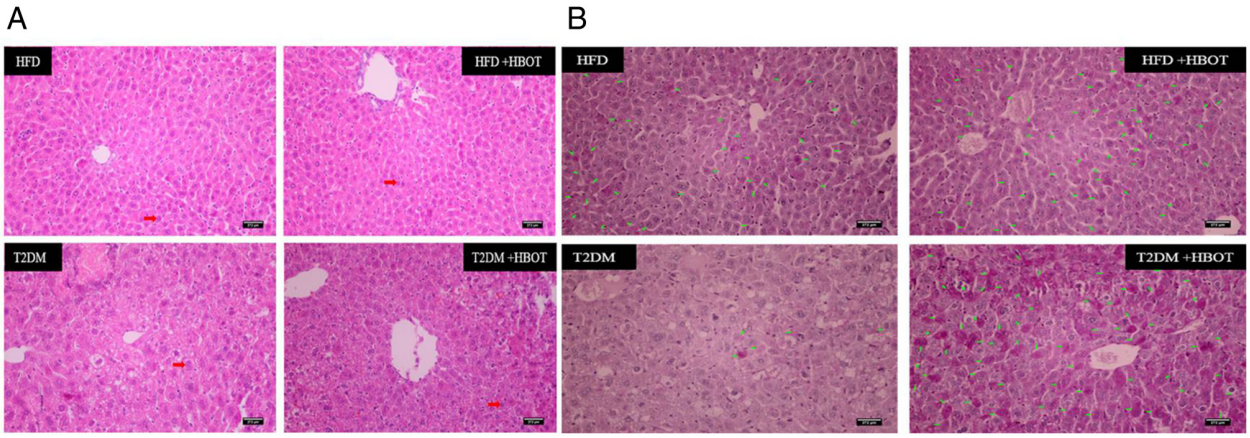

Figure 7. Effects of HBOT on hepatic gluconeogenesis. (A) Representative H&E staining of the liver (Scale bar, 272 μm). (B) Representative H&E staining of glycogen in the liver. Green arrows point to glycogen (Scale bar, 272 μm). HBO, hyperbaric oxygen; HFD, high-fat diet; HBOT, hyperbaric oxygen therapy; T2DM, type-2 diabetes mellitus.

hepatocytes appeared more orderly after HBOT, and there were fewer intracytoplasmic vacuoles and inflammatory cells. The nuclei were larger and located in the center, and there was less shrinkage and necrosis than in the T2DM group (Fig. 7A). HBOT increased hepatic glycogen storage in T2DM mice (Fig. 7B).

Discussion

Diabetes mellitus has emerged as a significant public health issue worldwide, and T2DM is a common type of diabetes, accounting for 90-95% cases (27). Environmental and genetic factors cause β-cell dysfunction and insulin resistance (28), with hyperglycemia and lipid metabolism disorders as the main symptoms. Hyperglycemia may affect the function of tissues and organs, including the kidneys, eyes and the nervous system (29), if not controlled by medical, nutritional or physical interventions (30). The complications of T2DM result in severe health and social problems if untreated or mishandled, eventually reducing the quality of life and life span of patients (31).

Insulin resistance and β-cell dysfunction are responsible for hyperglycemia in T2DM and can result in numerous metabolic abnormalities (32,33). Insulin resistance is an inadequate biological response to target tissue insulin stimulation, such as the liver, muscle and adipose tissue (34). Insulin resistance impairs glucose metabolism, resulting in compensatory increases in β-cell insulin production and hyperinsulinemia (35). The causes of insulin resistance include obesity, diabetes and physical inactivity, although there may also be genetic factors (36). Therefore, the mechanisms involved in the development of insulin resistance are multifactorial.

HBO therapy is a relatively safe and non-invasive treatment that has been applied in various diseases, including diabetic patients with non-healing foot ulcers (8). HBOT has also been reported to reduce FBG and increased insulin sensitivity (10,11). Our previous study also demonstrated consistent results. In T2DM mice, HBOT improved insulin sensitivity by activating muscle Akt protein phosphorylation to promote GLUT4 expression (13). Skeletal muscle serves an essential role in regulating blood glucose, accounting for ~75% of total glucose

clearance (37). In type-1 diabetes mellitus (T1DM) model mice, HBOT improved glucose metabolism by protecting islet β-cells and enhancing hepatic glycogen storage (19).

The liver is another vital organ for glucose metabolism and energy balance. In a fasting state, hepatic gluconeogenesis fills the need for glucose by the brain. By contrast, the liver stores glucose as glycogen or fat while in the fed state (38). Faleo *et al* (39) reported that HBOT preserved islet β-cell mass by stimulating proliferation, inhibiting apoptosis and suppressing insulitis in non-obese diabetic mice. Therefore, the present study focused on the effects of HBOT on blood glucose, pancreas β-cell state and hepatic glycogen storage in T2DM mice. Due to the limited application of HBOT in diabetes, previous studies are limited, and the effect of HBOT on diabetes requires further study.

In the present study, the T2DM and T2DM+HBOT were established as the experimental groups, and the HFD and HFD+HBOT groups were established as the control groups. A key limitation of the present study was lack of a normal diet group, which would have been more rigorous.

The successful T2DM model establishment rate was 100%, and no mice died during model establishment. Both non-FBG and FBG levels of the T2DM group were higher compared with those in the HFD group, suggesting the success of T2DM model establishment. As the success rate of T2DM modeling is unknown at first, the sample size of the T2DM group was doubled in order to reduce sampling error and improve statistical efficiency. The current results showed that the rate of successful T2DM model-building was 100%, so the sample size of the T2DM group and the HFD group were different, which is another limitation of the present study.

After establishing the T2DM model, HBOT (2.0 ATA, 100% O_2, 1 h per day) was administered for 7 consecutive days. During HBOT, 12-h nocturnal food intake was measured every day to investigate the effects of HBOT on nocturnal food intake, but no remarkable differences among the HBOT groups were identified. The feeding results were inconsistent with our previous work, which indicated that HBOT increased the cumulative food intake in the last 12 h in T2DM mice (13). This difference may be due to the method of monitoring. As for the 7-day body weight, there were no significant differences among the four groups, and HBOT did not markedly reduce the body weight gain on the 8th day in both the HFD and T2DM groups. After sacrifice, fat mass, including inguinal subcutaneous adipose tissue and visceral epididymal adipose tissue, was measured. HBOT decreased inguinal fat, and the sum of inguinal fat and epididymal fat in T2DM mice, potentially via increasing fat utilization, accelerating fat metabolism and reducing fat accumulation in diabetic mice.

HBOT significantly reduced peak blood glucose levels at 15 min and the area under the blood glucose curve within 120 min of IPGTT in T2DM mice. These findings suggested that HBOT improved glucose tolerance in T2DM mice. Subsequently, HOMA-IR and HOMA-β were calculated to assess insulin resistance and β-cell function, respectively. The HOMA-IR of T2DM mice was significantly higher compared with that of HFD mice, indicating that T2DM mice displayed severe insulin resistance. The HOMA-IR was significant reduced in the T2DM+HBOT group compared with that in the T2DM group, indicating that HBOT significantly improved insulin sensitivity. The HOMA-β results suggested that β-cell function in the T2DM group was significantly lower compared with that in the HFD group. However, HBOT did not have a significant therapeutic effect on β-cell function in T2DM mice.

The H&E staining results showed that HBOT significantly increased large islets (>10 cells). Both β-cell area and β-cell mass were increased in the pancreatic tissue after HBOT in the T2DM mice. Although there was no significant therapeutic effect between the HFD groups, a therapeutic trend consistent with those in the T2DM groups was observed following HBOT. Moreover, β-cell area in the T2DM group was significantly smaller compared with that in the HFD group, and the β-cell mass in the T2DM group was significantly lower compared with that in the HFD group. These results indicated that the β-cell morphology and structure were more severely damaged in T2DM mice compared with those in HFD mice, which provided a potential explanation for the lack of significant therapeutic effect in the HFD+HBOT group.

To investigate the underlying mechanism, the TUNEL assay was used to measure the effects of HBOT on pancreatic β-cell apoptosis. HBOT significantly reduced the apoptotic rate in T2DM mice, confirming the findings of Faleo *et al* (39). Subsequently, apoptotic protein expression levels were measured. The results indicated that HBO reduced the β-cell apoptotic rate via the pancreatic Bcl-2/caspase-3/PARP apoptosis pathway in T2DM mice. By contrast, Matsunami *et al* (40) demonstrated that HBO exposure induced pancreas apoptosis in STZ-induced diabetic rats. However, the present study investigated the effects of HBOT on T2DM mice, whereas Matsunami *et al* used T1DM model rats. Therefore, further research is required to confirm these results.

The liver is an essential organ in glucose metabolism (38). Our previous study demonstrated that HBOT enhanced hepatic glycogen storage in T2DM mice (19). The results of the present study suggested that HBO improved the structure of hepatocytes and increased hepatic glycogen storage in T2DM mice.

In conclusion, examining the underlying mechanism for pancreatic β-cell apoptosis is crucial for understanding the pathogenesis of diabetes. To the best of our knowledge, the present study was the first to report that HBOT increased insulin sensitivity by reducing β-cell apoptosis via the pancreatic Bcl-2/caspase-3/PARP apoptosis pathway in T2DM mice, which suggested that HBOT may represent a potential treatment for patients with T2DM.

Acknowledgements

The authors would like to thank Miss Yuan Liu and Miss Li-min Song (Qingdao University, China) for taking care of the mice during HBOT in the experiments.

Funding

The present study was supported by the National Natural Science Foundation of China (grant no. 31872791) and the

Science Foundation of Shandong Province of China (grant no. ZR201807070189).

Availability of data and materials

The datasets used and/or analyzed during the current study are available from the corresponding author on reasonable request.

Authors' contributions

CZ and DZ confirm the authenticity of all the raw data. JD, GG, CZ and DZ conceived and designed the study. CZ, DZ, HW, QL, ML and JY performed the experiments. CZ and DZ analyzed the data. CZ, DZ and JD drafted the manuscript. JD, CZ, DZ and GG reviewed and edited the manuscript, and gave final approval of the version to be published. All authors have read and approved the final manuscript.

Ethics approval and consent to participate

The experimental protocols were approved by the Qingdao University Animal Care and Use Committee and Animal Welfare Committee (approval no. QYFY WzLL26594) in accordance with the National Institutes of Health guidelines.

Patient consent for publication

Not applicable.

Competing interests

The authors declare that they have no competing interests.

References

1. Cho NH, Shaw JE, Karuranga S, Huang Y, da Rocha Fernandes JD, Ohlrogge AW and Malanda B: IDF diabetes atlas: Global estimates of diabetes prevalence for 2017 and projections for 2045. Diabetes Res Clin Pract 138: 271-281, 2018.
2. Lu Y, Li Y, Li G and Lu H: Identification of potential markers for type 2 diabetes mellitus via bioinformatics analysis. Mol Med Rep 22: 1868-1882, 2020.
3. Ichise M and Harris PE: Imaging of beta-cell mass and function. J Nucl Med 51: 1001-1004, 2010.
4. DeFronzo RA, Eldor R and Abdul-Ghani M: Pathophysiologic approach to therapy in patients with newly diagnosed type 2 diabetes. Diabetes Care 36 (Suppl 2): S127-S138, 2013.
5. Weir GC and Bonner-Weir S: Islet β cell mass in diabetes and how it relates to function, birth, and death. Ann N Y Acad Sci 1281: 92-105, 2013.
6. Butler AE, Janson J, Bonner-Weir S, Ritzel R, Rizza RA and Butler PC: Beta-cell deficit and increased beta-cell apoptosis in humans with type 2 diabetes. Diabetes 52: 102-110, 2003.
7. Germonpre P, Levie P, Dehalleux C and Caers D: ENT indications for Hyperbaric Oxygen Therapy. B-ENT Suppl 26: S87-S106, 2016.
8. Karadurmus N, Sahin M, Tasci C, Naharci I, Ozturk C, Ilbasmis S, Dulkadir Z, Sen A and Saglam K: Potential benefits of hyperbaric oxygen therapy on atherosclerosis and glycaemic control in patients with diabetic foot. Endokrynol Pol 61: 275-279, 2010.
9. Chen CY, Wu RW, Hsu MC, Hsieh CJ and Chou MC: Adjunctive hyperbaric oxygen therapy for healing of chronic diabetic foot ulcers: A randomized controlled trial. J Wound Ostomy Continence Nurs 44: 536-545, 2017.
10. Wilkinson D, Nolting M, Mahadi MK, Chapman I and Heilbronn L: Hyperbaric oxygen therapy increases insulin sensitivity in overweight men with and without type 2 diabetes. Diving Hyperb Med 45: 30-36, 2015.
11. Wilkinson D, Chapman IM and Heilbronn LK: Hyperbaric oxygen therapy improves peripheral insulin sensitivity in humans. Diabet Med 29: 986-989, 2012.
12. Nagatomo F, Takemura A, Roy RR, Fujino H, Kondo H and Ishihara A: Mild hyperbaric oxygen inhibits the growth-related decline in skeletal muscle oxidative capacity and prevents hyperglycemia in rats with type 2 diabetes mellitus. J Diabetes 10: 753-763, 2018.
13. Liu Y, Zhang D, Yuan J, Song L, Zhang C, Lin Q, Li M, Sheng Z, Ma Z, Lv F, *et al*: Hyperbaric oxygen ameliorates insulin sensitivity by increasing GLUT4 expression in skeletal muscle and stimulating UCP1 in brown adipose tissue in T2DM mice. Front Endocrinol (Lausanne) 11: 32, 2020.
14. Jansson L and Hellerström C: Stimulation by glucose of the blood flow to the pancreatic islets of the rat. Diabetologia 25: 45-50, 1983.
15. Kleinert M, Clemmensen C, Hofmann SM, Moore MC, Renner S, Woods SC, Huypens P, Beckers J, de Angelis MH, Schürmann A, *et al*: Animal models of obesity and diabetes mellitus. Nat Rev Endocrinol 14: 140-162, 2018.
16. Yu T, Sungelo MJ, Goldberg IJ, Wang H and Eckel RH: Streptozotocin-treated high fat fed mice: A new type 2 diabetes model used to study canagliflozin-induced alterations in lipids and lipoproteins. Horm Metab Res 49: 400-406, 2017.
17. Yuan J, Jiang Q, Song L, Liu Y, Li M, Lin Q, Li Y, Su K, Ma Z, Wang Y, *et al*: L-Carnitine is involved in hyperbaric oxygen-mediated therapeutic effects in high fat diet-induced lipid metabolism dysfunction. Molecules 25: 176, 2020.
18. Zhang D, Yu YJ, Xu FS, Yuan JH, Wang R, Zhang CS, Wang LX, Liu Y, Song LM, Liu JL and Dong J: Recombinant betatrophin (Angptl-8/lipasin) ameliorates streptozotocin-induced hyperglycemia and β-cell destruction in neonatal rats. Mol Med Rep 20: 4523-4532, 2019.
19. Song L, Yuan J, Liu Y, Zhang D, Zhang C, Lin Q, Li M, Su K, Li Y, Gao G, *et al*: Ghrelin system is involved in improvements in glucose metabolism mediated by hyperbaric oxygen treatment in a streptozotocin-induced type 1 diabetes mouse model. Mol Med Rep 22: 3767-3776, 2020.
20. Jensen TL, Kiersgaard MK, Sørensen DB and Mikkelsen LF: Fasting of mice: A review. Lab Anim 47: 225-240, 2013.
21. Wei X, Gu N, Feng N, Guo X and Ma X: Inhibition of p38 mitogen-activated protein kinase exerts a hypoglycemic effect by improving β cell function via inhibition of β cell apoptosis in db/db mice. J Enzyme Inhib Med Chem 33: 1494-1500, 2018.
22. Cui X, Wang B, Wu Y, Xie L, Xun P, Tang Q, Cai W and Shen X: Vegetarians have a lower fasting insulin level and higher insulin sensitivity than matched omnivores: A cross-sectional study. Nutr Metab Cardiovasc Dis 29: 467-473, 2019.
23. Kou K, Saisho Y, Satoh S, Yamada T and Itoh H: Change in β-cell mass in Japanese nondiabetic obese individuals. J Clin Endocrinol Metab 98: 3724-3730, 2013.
24. Lautenbach A, Wernecke M, Riedel N, Veigel J, Yamamura J, Keller S, Jung R, Busch P, Mann O, Knop FK, *et al*: Adaptive changes in pancreas post Roux-en-Y gastric bypass induced weight loss. Diabetes Metab Res Rev 34: e3025, 2018.
25. Poret JM, Souza-Smith F, Marcell SJ, Gaudet DA, Tzeng TH, Braymer HD, Harrison-Bernard LM and Primeaux SD: High fat diet consumption differentially affects adipose tissue inflammation and adipocyte size in obesity-prone and obesity-resistant rats. Int J Obes (Lond) 42: 535-541, 2018.
26. Siersbæk MS, Ditzel N, Hejbøl EK, Præstholm SM, Markussen LK, Avolio F, Li L, Lehtonen L, Hansen AK, Schrøder HD, *et al*: C57BL/6J substrain differences in response to high-fat diet intervention. Sci Rep 10: 14052, 2020.
27. Faselis C, Katsimardou A, Imprialos K, Deligkaris P, Kallistratos M and Dimitriadis K: Microvascular complications of type 2 diabetes mellitus. Curr Vasc Pharmacol 18: 117-124, 2020.
28. Stumvoll M and Gerich J: Clinical features of insulin resistance and beta cell dysfunction and the relationship to type 2 diabetes. Clin Lab Med 21: 31-51, 2001.
29. Elosta A, Ghous T and Ahmed N: Natural products as anti-glycation agents: possible therapeutic potential for diabetic complications. Curr Diabetes Rev 8: 92-108, 2012.
30. Guo S: Insulin signaling, resistance, and the metabolic syndrome: insights from mouse models into disease mechanisms. J Endocrinol 220: T1-T23, 2014.
31. Utumatwishima JN, Chung ST, Bentley AR, Udahogora M and Sumner AE: Reversing the tide-diagnosis and prevention of T2DM in populations of African descent. Nat Rev Endocrinol 14: 45-56, 2018.

32. DeFronzo RA, Ferrannini E, Groop L, Henry RR, Herman WH, Holst JJ, Hu FB, Kahn CR, Raz I, Shulman GI, *et al*: Type 2 diabetes mellitus. Nat Rev Dis Primers 1: 15019, 2015.
33. Kitamura T: The role of FOXO1 in β-cell failure and type 2 diabetes mellitus. Nat Rev Endocrinol 9: 615-623, 2013.
34. Freeman AM and Pennings N: Insulin Resistance. In: StatPearls (Internet). Treasure Island, FL, 2021. https://www.ncbi.nlm.nih.gov/books/NBK507839. Accessed July 10, 2021.
35. Hjermann I: The metabolic cardiovascular syndrome: Syndrome X, Reaven's syndrome, insulin resistance syndrome, atherothrombogenic syndrome. J Cardiovasc Pharmacol 20 (Suppl 8): S5-S10, 1992.
36. Stumvoll M and Häring H: Insulin resistance and insulin sensitizers. Horm Res 55 (Suppl 2): 3-13, 2001.
37. Klip A and Pâquet MR: Glucose transport and glucose transporters in muscle and their metabolic regulation. Diabetes Care 13: 228-243, 1990.
38. Rui L: Energy metabolism in the liver. Compr Physiol 4: 177-197, 2014.
39. Faleo G, Fotino C, Bocca N, Molano RD, Zahr-Akrawi E, Molina J, Villate S, Umland O, Skyler JS, Bayer AL, *et al*: Prevention of autoimmune diabetes and induction of β-cell proliferation in NOD mice by hyperbaric oxygen therapy. Diabetes 61: 1769-1778, 2012.
40. Matsunami T, Sato Y, Hasegawa Y, Ariga S, Kashimura H, Sato T and Yukawa M: Enhancement of reactive oxygen species and induction of apoptosis in streptozotocin-induced diabetic rats under hyperbaric oxygen exposure. Int J Clin Exp Pathol 4: 255-266, 2011.